Journal of Ocean and Wind Energy (ISSN 2310-3604)

Vol. 2, No. 1, February 2015, pp. 12–20

http://www.isope.org/publications

Comparison of Experimental Results and Computations for Tension-Leg-Buoy Offshore Wind Turbines

Anders Myhr
Department of Mathematical Sciences and Technology, Norwegian University of Life Sciences (NMBU)
Ås, Norway

Tor Anders Nygaard
Energy Systems Department, Institute for Energy Technology (IFE)
Kjeller, Norway

This work compares wave tank experimental results in scale 1:40 and hydro-elastic computations of three different Tension-Leg-Buoy (TLB) offshore wind turbine platforms. The results include comparisons of time-series of displacements for free-decay tests, time-series of tower top motion and mooring line tension for selected regular wave cases, Power Spectral Densities (PSD) for one irregular wave case, and Response Amplitude Operators (RAO) for tower top motion and mooring line tension for all the regular and the irregular wave cases. The experimental results and computations agree well, and both capture interactions between hydrodynamic loading, flexible motion of the floater/tower, and the tower top motions. The time series of the experimental results will be publicly available for further development and validation of computational tools for offshore wind turbine platforms.

INTRODUCTION

Several new floating offshore wind turbine concepts are under development. Some commonly known examples are the SWAY Tension-Leg-Spar (Karimirad and Moan, 2013), the full-scale WindFloat system (Roddier et al., 2010), and the HYWIND system (Tande et al., 2014), where a single turbine has been operating full-scale since 2009. Several concepts are also in the early prototype development stage, such as different Tension-Leg-Buoy (TLB) and Tension-Leg-Platform (TLP) systems, but trials for these concepts have so far been limited to wave basins (Myhr and Nygaard, 2012; Robertson and Jonkman, 2011; Stewart et al., 2012; Copple and Capanoglu, 2012).

The evolution from onshore to offshore bottom-fixed wind turbines increases computational complexity through the inclusion of wave loading and the need for more complex soil models. Floating structures such as TLPs and TLBs have similarities to bottom-fixed structures due to the stiff mooring system. Nevertheless, they represent another level of complexity because of mooring lines and larger motions. Finally, large floaters like semisubmersibles need consideration of detailed hydrodynamic models to account for effects such as diffraction and radiation. “Floater” here refers to the part of the substructure below the tower/floater interface, typically at 10 m above the still water line in full scale. Due to the large number of load cases (LC) needed to check the feasibility of a design, computational tools must be efficient. In addition, high accuracy is necessary to reduce the risk of failure and to achieve a cost-optimized design.

The International Energy Agency (IEA) Wind Task 23 projects known as Offshore Code Comparison Collaboration (OC3) (Jonkman et al., 2010) and the follow-up project OC4 (Popko et al., 2012) are important drivers for the development and verification of computational tools for offshore wind turbines. The lack of publicly available experimental results means the activity so far has been limited to verification through comparisons of computational results from different codes. In the ongoing OC5 project, model validations against wave tank results and full-scale data are just starting. The FAST code (Jonkman, 2007) was recently validated against experimental results for a TLP platform. It produced good results but also discrepancies that could not be explained at the time (Stewart et al., 2012). In order to support model validation, we recently conducted wave tank experiments on three different TLB floaters at the IFREMER wave tank in Brest, France through the MARINET project. In this paper, we compare some of the results with corresponding computations with the in-house simulation tool 3DFloat at IFE.

APPROACH

The experimental results herein include time series of wave height, tower top motion, and mooring line tension, as well as video recordings. The LCs include decay tests and regular- and irregular-wave cases (Myhr and Nygaard, 2014). For a full-scale floater, most of the wave excitation is in the range 0.05 to 0.2 Hz, corresponding to 0.3 to 1.3 Hz for the 1:40 scale model. The results are presented as PSDs and RAOs. For the RAO computations, the absolute value of the Fourier amplitude of the response is divided by the absolute value of the Fourier amplitude of the wave height.

The comparisons are performed in three steps:

(1) Decay tests: They are particularly useful for checking the modeling of the structural and added mass, plus the stiffness of the mooring system, through comparison of the eigenperiods. The obtained damping ratios allow tuning of the parameters affecting the damping, such as the drag coefficient in the Morison force model, linear damping applied to the floater, the hysteresis damping applied to the fairleads, and structural damping in the mooring lines.

(2) Regular wave cases: From these one can make direct and detailed comparisons of time series results, peaks and amplitudes for both motions, and mooring line tension.

Received July 24, 2014; revised manuscript received by the editors December 23, 2014. The original version was submitted directly to the Journal.
KEY WORDS: Offshore wind turbine, experimental results, Tension-Leg-Buoy (TLB), hydro-elastic computations.

(3) Irregular wave cases: These are presented with PSDs and RAOs in order to give a quick overview of the platform responses to loading with a combination of different frequencies.

COMPUTATIONAL TOOL

3DFloat is an aero-servo-hydro-elastic simulation tool developed at IFE and NMBU for the computation of dynamic response of elastic structures subject to combined wind and wave loading, such as offshore wind turbines and suspension bridges (Myhr and Nygaard, 2012). It is coded in FORTRAN90 with linear algebra routines from the LAPACK library (Anderson et al., 1990).

The core is a general nonlinear Finite Element Method (FEM) framework. The load models include hydrodynamics and rotor aerodynamics. 3DFloat is one of the tools verified with the OC3-Hywind floating wind turbine in the IEA OC3 project (Vorpahl et al., 2013), the bottom-fixed space-frame ("Jacket") in the IEA OC4 project (Popko et al., 2012), and the semisubmersible platform in the IEA OC4 project (Robertson et al., 2014). An optimization example and further details of the model are given in Myhr and Nygaard (2012).

EXPERIMENTAL SETUP

The data sets utilized for validation in this work were obtained in experiments in the IFREMER wave tank in Brest, France. The experimental data and setup are described in a separate paper (Myhr and Nygaard, 2014). An overview of the setup is shown in Fig. 1 and Fig. 2.

Simplifications

The main simplification of the geometry in the Simulation Model (SM) is ignoring the fairlead brackets (with a mass of 0.022 kg and dimensions of 20 mm by 30 mm). The sum of the mass for all brackets amounts to about 0.150 kg. The SM beam model has rigid, massless connectors from the center of the floater to the fairleads. The connectors for the Physical Model (PM) are small 50 mm stainless carabiners, each about 0.01 kg.

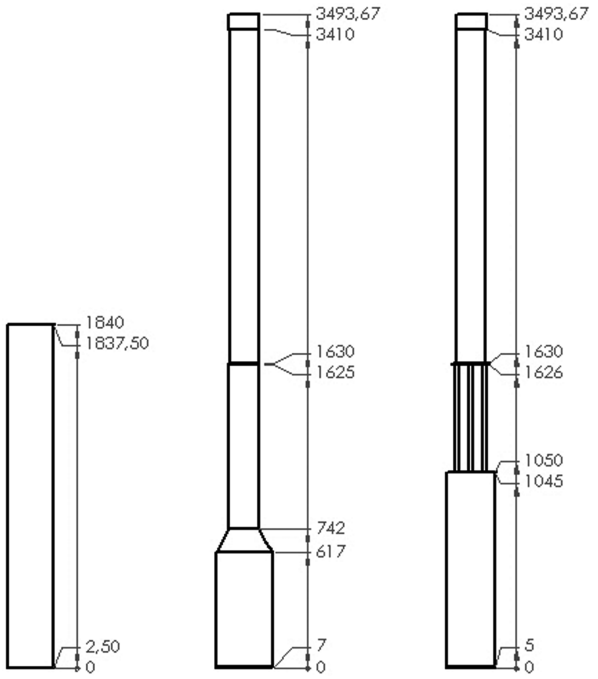

Fig. 1 Sketches of the selected geometries (from left to right): TLB S, TLB B, and TLB X3. The indicated height levels [mm] correspond to transitions in mass and/or diameter (Spæren, 2013).

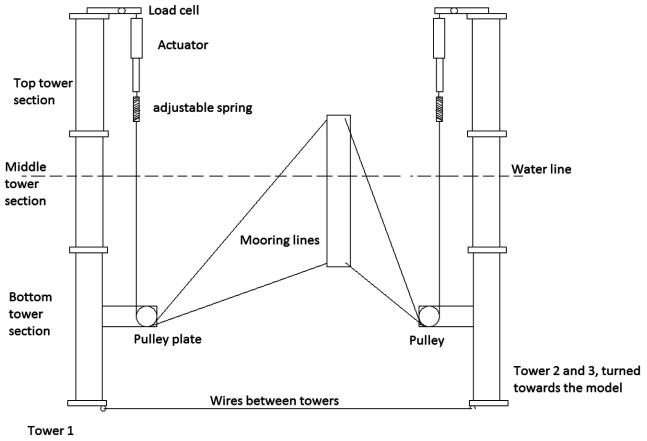

Fig. 2 Experimental setup with load cell, actuator, pulleys, and supporting towers. A spacing wire between the towers is shown, but additional pretension wires have been removed for clarity (Spæren, 2013).

	LC 1	LC 2	LC 3	LC 4	LC 5*
Period [s]	3.04	1.58	3.04	2.53	1.26
Hs [m]	0.28	0.13	0.28	0.28	0.08
Gamma	1.05	2.87	1.05	2	1.05

*LC 5 was only run with TLB X3

Table 1 The irregular LC Jonswap spectrums. LC 1 and LC 3 have identical wave characteristics in order to check the consistency of the test.

H [m]\Period [s]	0.95	1.26	1.58	1.8	2.5	2.8*
0.13	LC 6	LC 7	LC 9	LC 11	—	LC 15
0.3	—	LC 8	LC 10	LC 12	—	LC 16
0.5	—	—	—	LC 13	LC 14	LC 17

*LC only run on TLB X3

Table 2 Regular wave load conditions

Load Cases

Tables 1 and 2 show the irregular- and regular-wave LCs of the experiment. Detailed comparisons are performed for the regular-wave cases LC 9 and LC 12, and the irregular wave case LC 1. The regular and the irregular cases are then compared with RAOs.

Figure 3 shows comparisons of the wave spectrums in the experiment and the computations. The five-minute runs in the wave tank correspond to 30 minutes in full scale. This results in some differences in wave spectums between different realizations, as seen for LC 1 vs. LC 3. The simulation model was run with superposition of linear Airy waves, corresponding to the characteristics of Table 1, with a simulation length corresponding to 80 minutes in full scale. The differences in excitation between the experiment and model are, to some degree, accounted for when computing RAOs.

MODEL CONSTANTS

The spectral radius for the generalized α-method was set to 0.9. Compared to a spectral radius of 1.0 (corresponding to the

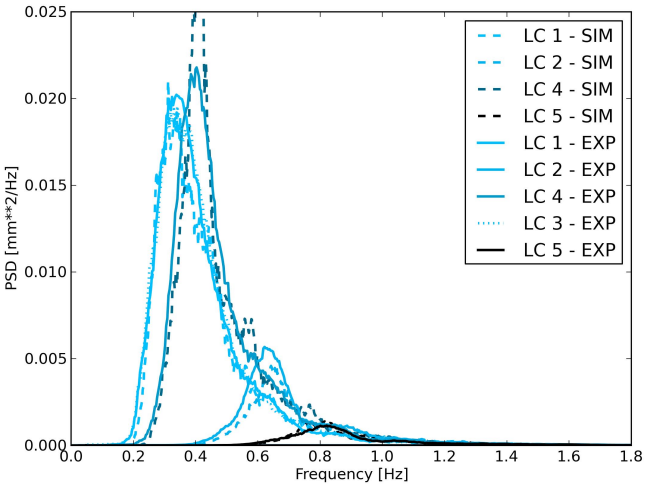

Fig. 3 Wave spectrums from both the simulations (-) and the experimental trials (–)

Newmark method), this gives an algorithmic damping of high-frequency noise, which we found improved the convergence without changing the computed forces. The Rayleigh structural damping model coefficients were chosen to give 1% of critical damping in the floater and tower between 0.3 and 1.3 Hz. The drag and inertia coefficients (C_d and C_m) in the relative form of the Morison equation were chosen as a function of the Keulegan-Carpenter (KC) and oscillatory Reynolds numbers (Re) from experimental data (Sarpkaya and Isaacson, 1981). For LC 9, KC at the still water level (MSL) are 1.6, 1.6, and 19 for TLB S, TLB B, and TLB X3, respectively. The values of Re are 36,000, 37,000, and 3,100. For LC 12, KC at the MSL are 3.8, 3.6, and 43 for TLB S, TLB B, and TLB X3, respectively. Corresponding Re are 73,000, 76,000, and 6,400. The slender cylinders penetrating the surface for TLB X3 have drag coefficients of 1.0 and inertia coefficients of 1.8. The TLB X3 floater body (below the space frame) has coefficients of 1.0 and 2.0 for drag and inertia, respectively, similar to the TLB B and TLB S. The axial drag coefficients for the bottom end caps are set to 2.0. This corresponds to a flat plate at 90-deg angle-of-attack, taking into account the cone for TLB B and the top lid for TLB X3. The value may seem high for TLB S, but the results are inertia-dominated and not sensitive to this parameter. The hysteresis damping force of the mooring line pulleys was determined from the experiment by slowly loading and unloading the mooring lines. There is no tuning involved in the selection of model constants described in this section.

Mooring Lines

The axial stiffness in the mooring lines is shown in Table 3. Table 4 shows the pre-tensions of the mooring lines in the experiment. The variation between mooring lines at the same height is due to the scale models not being vertical and/or not being centered between the anchor points. We do not take this into account in the simulations, where identical pre-tensions for mooring lines at the same height were used, as listed in Table 5. As long as tension is maintained in all mooring lines, the pre-tension level is not important for the taut mooring line stiffness and thereby the motions and force amplitudes.

	1	2	3	4	5	6
TLB B/S	2.899	2.842	2.870	2.341	2.320	2.299
TLB X3	2.494	2.479	2.425	2.312	2.325	2.234

Table 3 Axial stiffness calibration values [N/mm] for the mooring lines (Myhr and Nygaard, 2014)

	Line 1	Line 2	Line 3	Line 4	Line 5	Line 6
TLB B	164.80	164.10	159.70	188.89	184.26	178.66
TLB S	200.73	195.14	197.14	184.79	177.58	179.66
TLB X3	149.51	147.99	142.60	185.55	180.19	173.26

Table 4 Mooring line pre-tension [N] in the experiment (Myhr and Nygaard, 2014)

	Lower (1, 2, and 3)	Upper (3, 4, and 5)
TLB B	170.5 N (0.0160)	184.7 N (0.0177)
TLB S	195.0 N (0.0180)	178.3 N (0.0171)
TLB X3	147.5 N (0.0160)	180.0 N (0.0174)

Table 5 Mooring line pre-tension [N] in the simulations with equivalent pre-strain [mm/mm] shown in parentheses

Preliminary sensitivity studies indicate that small offsets in the initial orientation have limited influence on the computed displacement and line tension amplitudes. Nevertheless, this should be studied further as it may be relevant and important for full-scale prototypes.

Decay Trials and Model Tuning

To replicate the heave decay in the experiment, a small force was applied in the heave direction at the top of the nacelle before being removed. The results are shown in Fig. 4. The computed heave decay was tuned manually by adjusting linear vertical damping applied at one node at the MSL, with final values of 23.0, 25.0, and 23.0 Ns/m for TLB B, TLB S, and TLB X3, respectively.

The heave periods were tuned by adjusting the axial added mass coefficient for the end caps in order to match the heave period in the experiment. This resulted in an axial added mass of 40% of a half-sphere of water on the bottom end cap and the tapered section for TLB B. The corresponding number for the bottom of TLB S is 25% and 55% for TLB X3 (sum of upper and lower end caps).

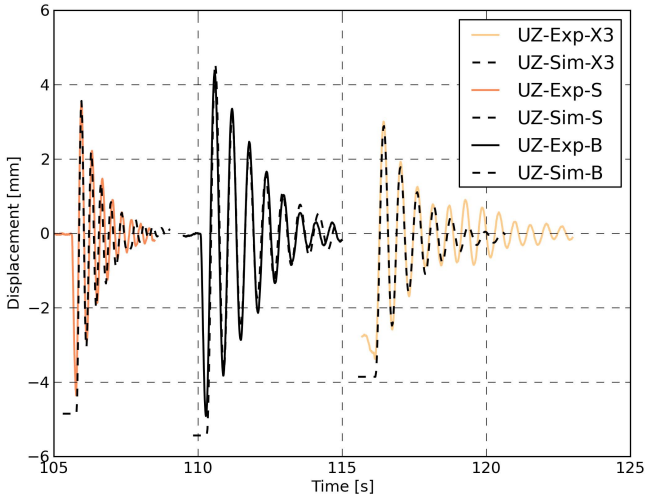

Fig. 4 Experiment heave decay tests for each of the physical models (PMs) compared to computations. The different PM time series are offset to allow presentation in the same figure.

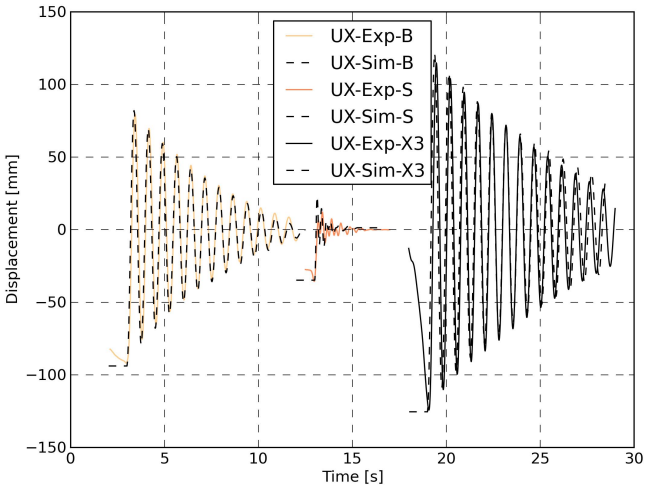

Fig. 5 Comparison of experimental pitch-surge decay data (continuous lines) and computations (dashed lines). The data shown are surge displacements.

The heave period for the experiment and computations, shown in Fig. 4, agree well for the first four cycles, where the amplitude decay is close to linear. In this part, the selected linear damping coefficients give good agreement between the experiment and simulations. The TLB X3 experimental results were disturbed by other modes after about 3 seconds. It was not possible to obtain a perfect heave excitation for X3 in the experiment, but the initial decay nevertheless allowed a tuning of the damping coefficient.

The second decay test was for coupled pitch and surge by exerting a temporary horizontal force on the nacelle. The stiffness-proportional coefficient in the Rayleigh structural damping model for the mooring lines was tuned manually in order to provide the best fit of the pitch/surge decay. The resulting values are 0.0023 s, 0.0050 s, and 0.0005 s for TLB B, TLB S, and TLB X3, respectively. The comparison of experiments and simulations is shown in Fig. 5.

For TLB B and TLB X3, the computed pitch-surge periods are marginally longer than in the experiment. The damping progression agrees well. TLB S, the floater with the lowest mass, has the same mooring system as TLB B, giving significantly shorter eigenperiods, as well as problems in the decay test with small amplitudes and interference from other modes. The period matches well, but the damping in the experiment is hard to interpret due to very small deflections. Overall, the decay tests can be simulated with high accuracy by 3DFloat.

The horizontal wave excitation in the SM is due to the inertia term and drag terms in Morison's equation, scaling with the inertia and drag coefficients, respectively. The heave excitation results from the axial inertia and drag terms in Morison's equation for the end caps, and the dynamic pressure on any surface with a vertical component in the surface normal, such as the bottom end caps, the transition from floater to space frame for TLB X3, and the conical section of TLB B. Due to the taut inclined mooring lines, the stiffness-controlled horizontal and vertical motions interact strongly.

Before embarking on the regular and irregular LCs, we carried out a sensitivity study by varying the Morison coefficients within a range of ±20% in the computations, while comparing the results with the experimental data. We did obtain a slight improvement in match by adjusting the Morison inertial coefficients, but we think the most robust approach is to select Morison coefficients as outlined earlier, tune damping and added mass in the decay tests, and to run the regular- and irregular-wave cases with these coefficients.

REGULAR WAVE TRIALS

The regular wave cases LC 9 and LC 12, shown in Tables 1 and 2, correspond to full-scale wave periods/heights of 10 s/5.2 m, and 11.4 s/12 m, respectively. The wave height to wavelength ratio is 0.03 and 0.06 for LC 9 and LC 12, respectively. The wave height to diameter ratio is above 1 for all floaters and LCs. The maximum diameter to wavelength ratio is 0.08. This means that the waves are non-breaking, small diffraction effects, and important viscous effects. Linear Airy wave theory and Morison's equation should be well suited for these computations. The waves in the simulations are generated by extrapolated Airy theory with a wave height corresponding to the value used as input to the experiment wave-maker. After ramping up the waves over 8 seconds, periodic results are typically obtained after 15 seconds of simulation time.

The periodic experimental results are extracted from the end of the run, due to severe transients when the first waves with large amplitudes hit the scale model. This is a trade-off between waiting out initial transients and growing reflections in the basin. Synchronization of the phases is achieved by an offset of the first wave in the computations.

LC 9: T = 1.58 s and H = 0.13 m (10 s and 5.2 m in full scale)

The simulations were run with regular waves with 2 seconds of initial stabilizing before H was ramped to the desired level over 8 seconds. Typically, few transients are expected for TLB systems, but in order to capture quasi-static, multi-harmonic behavior, ramped loading was found to be helpful. However, this is somewhat contradictory to the experiment where no ramping was used. Past experience was that the first two to three waves typically had a wave height of 120% to 150% of the desired wave height, resulting in a severe impact on the model and causing significant harmonic behavior. The problem of this effect was reduced by the selection of segments at the end of each trial's time domain, though with the compromise of increased reflections in the basin. The compared simulations and experimental results for LC 9 are shown in Figs. 4 to 6.

It is apparent that the heave amplitude and phase were computed quite well for all of the systems, although we experienced some multi-harmonic behavior in the computed heave for TLB S. The hysteresis damping in the pulleys, implemented as a friction hysteresis force applied on the fairlead in the computations, has a

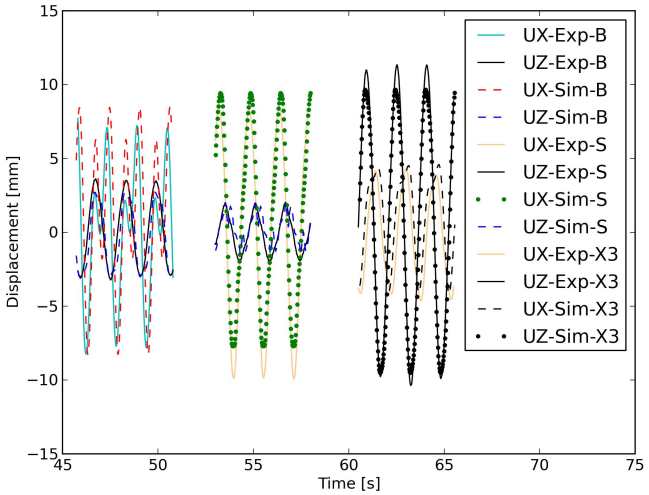

Fig. 6 Top displacement during LC 9 for all systems. Both surge (UX) and heave (UZ) are shown in the plot.

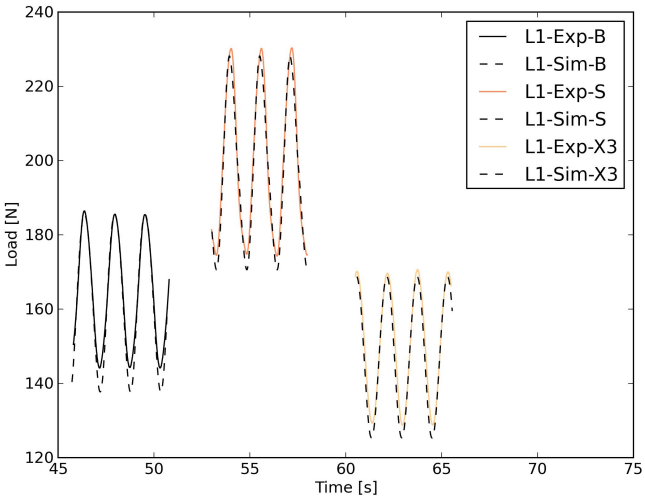

Fig. 7 Force in lower downstream mooring line during LC 9 for all systems

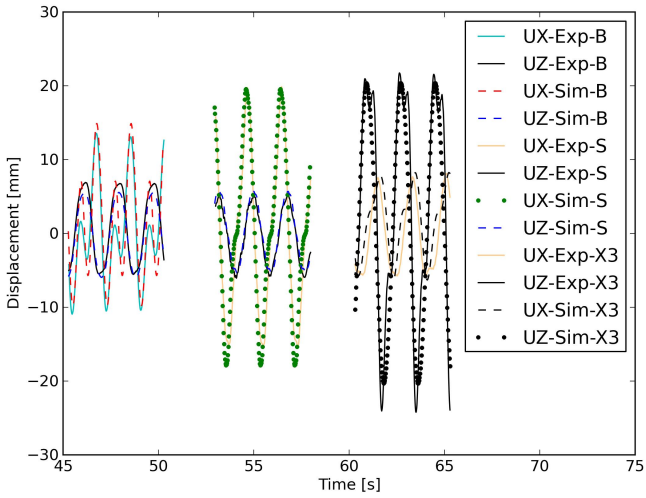

Fig. 9 Top displacement during LC 12 for all systems

significant influence. As the same pulley system was used for all the models, no modification to the hysteresis damping was attempted.

Displacement in pitch-surge is also computed quite well, especially for TLB S and TLB X3, with only minor offsets to the amplitude in the positive and negative directions, respectively. TLB B pitch-surge response is at the wave frequency and at twice the wave frequency (close to pitch-surge eigenfrequency), in both the experiment and the computations. An explanation for the discrepancy is that TLB B, for the regular cases with steep waves, never achieved a quasi-steady-state in the experiment, as one would expect for TLB designs during regular wave excitation. Typically, the pitch-surge eigenfrequency amplitude shifted from almost zero to the extremes, as shown in Fig. 6.

The lower mooring line forces are computed quite accurately for all models. An average discrepancy of less than 5 N, corresponding to less than 8% of the amplitude and less than 3% of the total load, is considered very good. The upper mooring force computations are also similar to the experiment, even with the relatively limited wave load excitations in LC 9. The mean offsets are due to differences in the initial setup in the model and experiment. Amplitudes for all of the models show a good match between the experiment and simulations, but the double frequency in TLB B influences the mooring line response in the computation somewhat more than indicated in the experiment.

The surge (UX) discrepancy for TLB B does not seem to influence the mooring loads significantly. Some discrepancies are observed for all of the PMs, but overall simulations compute results well within 10% of the measured values.

LC 12: T = 1.8 s and H = 0.3 m (11.4 s and 12 m in full scale)

The second regular LC features slight increases in both wave period and wave height. The compared results are shown in Figs. 9, 10, and 11. Slight multi-harmonic behavior is observed for TLB X3 in this case. The effect is present in both the simulation and the experiment. This is likely the result of pressure changes on the upper end cap of the floater. The heave and surge motions are somewhat influenced as a result of the change in added mass and thereby the resulting system inertia, but the experimental data are accurately replicated by the simulations. The surge motion in the experiment for TLB B and TLB S matches the simulations with no significant discrepancies. A slight overestimation of heave for TLB B is observed, while TLB S has an exact match.

The simulated lower mooring line forces are in line with the experiment. Discrepancies of 5% to 10% are observed for the

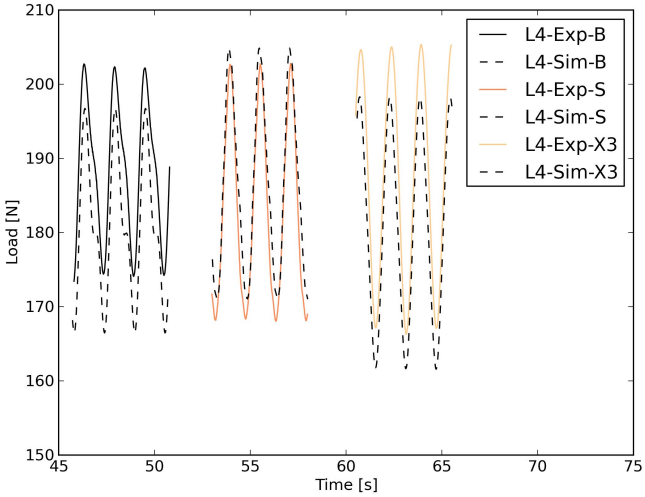

Fig. 8 Force in upper downstream mooring line during LC 9 for all systems

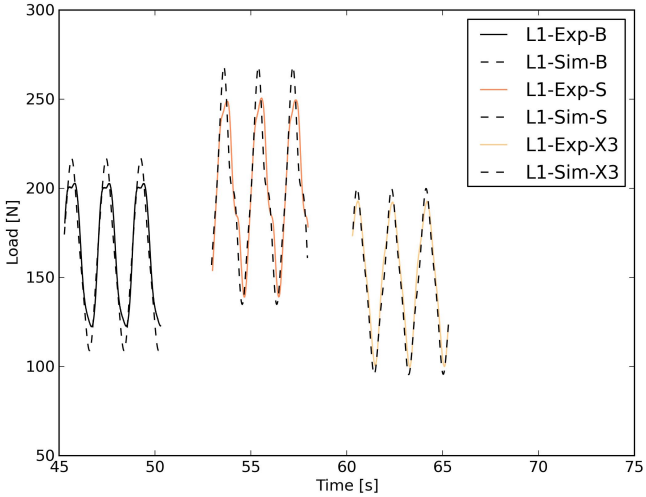

Fig. 10 Force in lower downstream mooring line during LC 12 for all systems

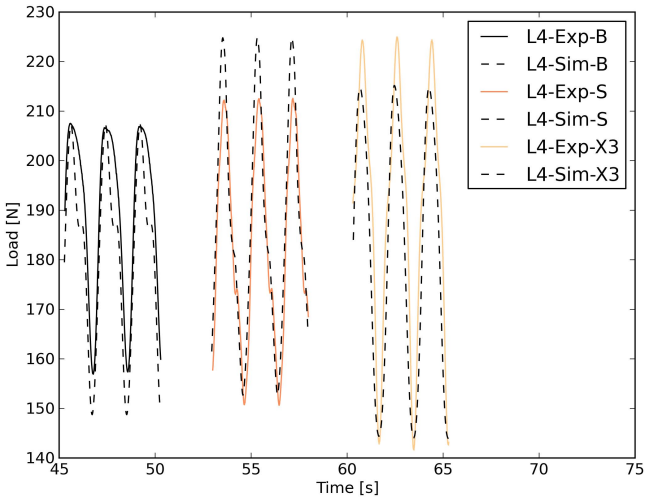

Fig. 11 Force in upper downstream mooring line during LC 12 for all systems

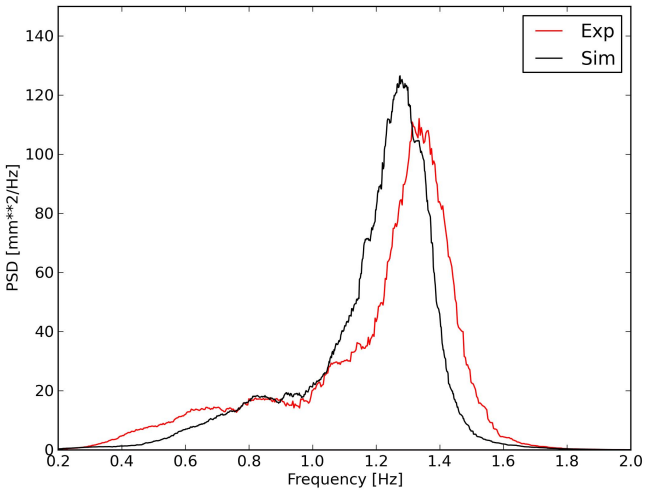

Fig. 12 PSD plot of pitch-surge motion for TLB B in LC 1

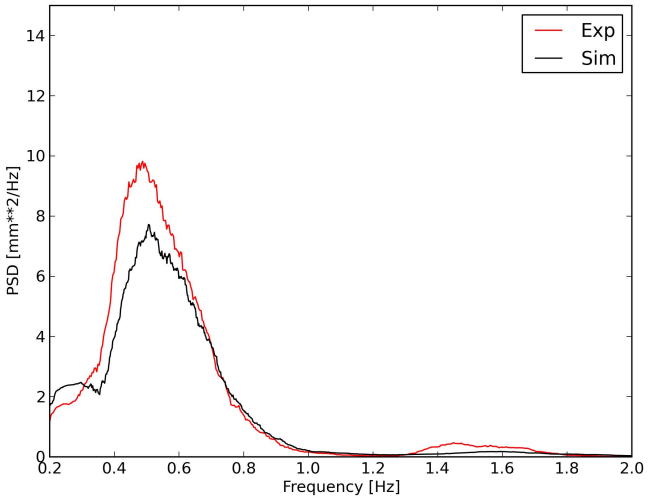

Fig. 13 PSD plot of heave motion for TLB B in LC 1

amplitudes for TLB B and TLB S. This corresponds to about 5% overestimation of the peak line force for TLB S. Nonlinear behavior can be noticed for TLB S. This is likely caused by the nonlinear damping occurring with larger deflections, which is noticed in the decay tests but is also captured by 3DFloat even if the amplitude is slightly off.

The observations of the upper mooring lines for LC 12 are similar to LC 9, but the double frequency is less pronounced in the simulations and is now negligible in the experiment. This is likely to be explained by a small difference in stiffness in the tower part of the model. The amplitudes are fairly in line for TLB B, but simulations overestimate the respective values for TLB S, while the values for TLB X3 are lower. Overall, the amplitudes deviate by $\pm 10\%$, while the total force is off by about $\pm 5\%$.

IRREGULAR WAVE TRIALS

In this section, one case is presented in detail with PSD on linear axes. This gives a visually intuitive interpretation of which frequencies contribute to the fluctuations of the selected response. All results from the regular and irregular LCs are then summarized by RAOs. For linear systems, where the response at one frequency is proportional to the excitation at the same frequency, RAOs are particularly useful. Despite the nonlinearities in this experiment, RAOs offers a first compact overview of the results, and it is interesting to see to what degree the results for one platform design fall on the same line, in order to get a sense of the linearity of the results. The RAO results of higher frequencies more than three times the wave peak frequency should be interpreted with caution. Here, the excitation is essentially zero, and the response is due to nonlinearities. Small absolute differences between the experiment and computations may be presented as large, noisy RAOs. In order to reduce noise for the RAOs, the plotted frequencies are collected from a limited range, depending on the LC. From LC 1 to LC 5, the intervals 0.2–0.8, 0.5–1.7, 0.2–0.8, 0.3–0.8, and 0.6–1.7 Hz are used, respectively.

Figure 12 shows the pitch-surge response for LC1. The differences up to 1 Hz can be partly explained by the differences in wave spectrums seen in Fig. 3. The pitch-surge motion response peak is at the pitch-surge eigenfrequency, despite the low wave excitation at this frequency, as also observed in LC 10 and LC 13. The resonant response is excited by nonlinearities. Figure 13 shows the PSD for the heave motion of TLB B. The wave peak frequency at 0.33 Hz shows up in the computations but not in the experiment. The peak just above 0.4 Hz corresponds roughly to the difference between the heave and pitch-surge eigenfrequencies, which have strong coupling through the mooring lines.

Figure 14 shows the first-order wave excitation and heave/pitch-surge difference frequencies dominating the lower mooring line response. The pitch-surge motion is mainly restricted by the upper mooring lines, as shown in Fig. 15. The upper mooring line response also shows a peak at the pitch-surge eigenfrequency.

It should also be noted that there is a discrepancy between the eigenfrequencies indicated in the simulation and the ones recorded in the experiment. As the decay tests produced very accurate responses, this is likely a result of the desired method of applying the hysteresis damping as friction on the fairleads in the computations. In the experiment, the physical introduction was through friction in the pulleys, corresponding to the full-scale anchor point. Small translations, as expected from high-frequency excitation, will then experience a higher stiffness from the mooring line wires because friction constrains the pulley.

The wave spectrums used in the computations shown in Fig. 3 are the same as the input to the wavemaker, with cut-offs at low frequencies determined by comparison with the measured wave spectrums, and high-frequency cut-offs at three times the wave peak frequencies. The experiment also shows minor wave

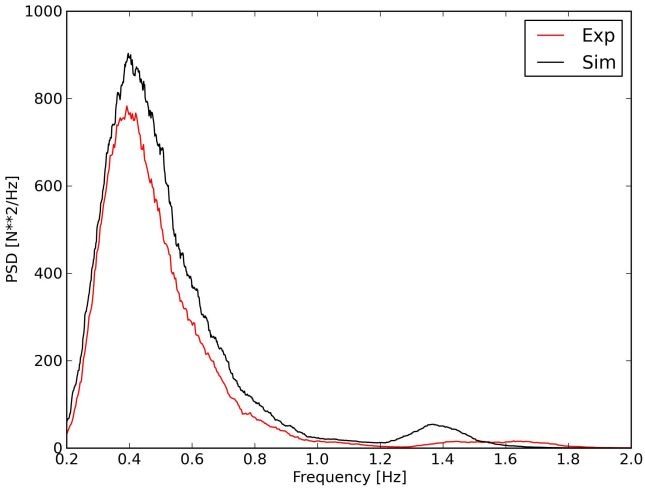

Fig. 14 PSD plot of lower downstream mooring line force for TLB B in LC 1

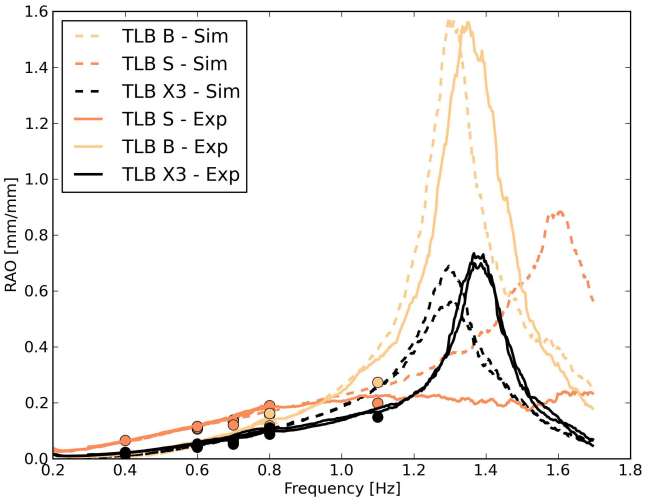

Fig. 16 RAOs for pitch-surge motion for all platforms, with regular cases represented as dots

reflections, from the model and the rig, in multiple directions that are not taken into account in the simulations.

The irregular wave trials were about 300 s each to limit the influence of wave reflections. The corresponding computations are 750 s long. Both the experiment and the simulations are too short to provide realization-independent spectrums. A new functionality in 3DFloat that allows time-accurate computations corresponding to the time-series of the measured waves is currently being implemented. This should reduce the uncertainty due to short wave realizations.

Figures 16 to 19 show RAOs of tower top pitch-surge motion, heave, and two mooring-line tensions for all cases, experiments, and computations. The irregular cases, except for LC 2 and LC 5, are cut off at 0.8 Hz to reduce clutter at high frequencies where the RAOs are less meaningful. For the pitch-surge motion, computations for TLB B produce excellent results both through the wave frequencies and around the pitch-surge eigenfrequency. Both TLB S and TLB X3 achieve good agreement below 1.0 and 0.8 Hz. TLB S deviates significantly at higher frequencies caused by the lack of damping, as discussed for LC 9. During shorter and steeper waves, significant turbulence and vortices are noticed downstream of the floater in addition to run-up due to the relatively large water plane area. This may further introduce nonlinear effects at higher frequencies. Due to the low mass, it is likely that the pitch-surge motion is damped out by effects that are not accounted for in 3DFloat, i.e., radiation damping. In addition, changes in water level and the low draft will influence the eigenfrequencies significantly. Since the results for TLB B, which utilizes the same mooring lines, are accurate, it is not likely that the mooring line stiffness is erroneous.

For TLB X3, the computations follow a smooth exponential curve, but the experimental results have a 0.1 Hz offset in the peak. This is significantly larger than the offset for TLB B. Four effects likely contribute to this result:

(1) The upper end cap in the floater is located close to the still water line. The waves influence the added mass and thereby influence both damping and eigenfrequencies. This is not modeled in the computations. The axial added mass associated with the upper end cap is either fully accounted for, or removed if the end cap comes out of the water.

(2) The stiffness of the mooring system is influenced differently from the pulley friction in the experiment and the computations, as explained earlier. Uncertainties in the measured mooring line stiffness also contribute to the discrepancies.

(3) The bending stiffness of TLB X3, in particular for the transition from end cap to the slim columns, is represented differently in

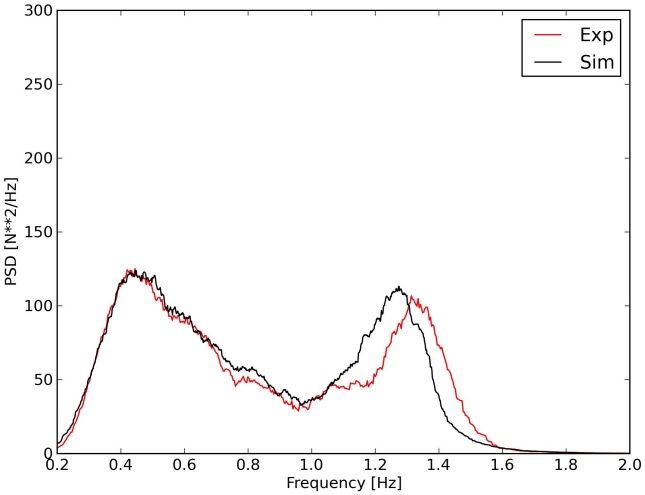

Fig. 15 PSD plot of upper downstream mooring line force for TLB B in LC 1

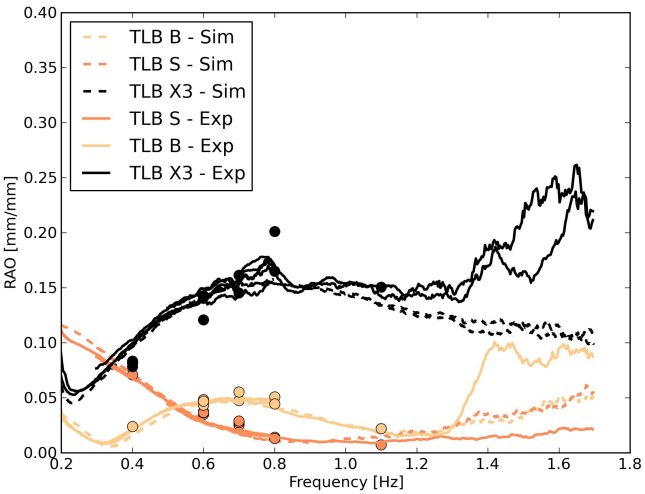

Fig. 17 RAOs in heave direction for all systems, with regular cases represented as dots

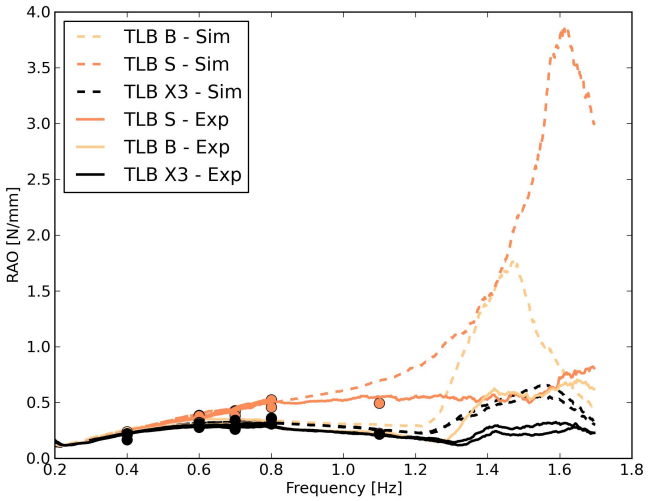

Fig. 18 RAOs for mooring line 1 tension (lower line, downstream direction) for all platforms, with regular cases represented as dots

the experiment scale model and the computations. The flexibility of the end cap is not taken into account in the computations. This may influence the decay tests and thereby the model setup of TLB X3.

(4) At higher frequencies, there will be changes in Re and KC values and thereby possible changes in the C_d and C_m coefficients. The previous sensitivity analyses were run on LC 9 and 12 only and established that a slight change in the coefficients was of less significance. However, the relevance of these, especially for the transition columns, becomes more important with higher frequencies and a corresponding increase in the relative part of the wave action zone affecting these elements. Further sensitivity analysis for the LCs with higher frequencies is therefore suggested.

In the results for heave, the peaks around 0.7 Hz and 1.6 Hz for TLB B and TLB X3 are due to the heave/pitch-surge difference frequency seen in Fig. 12, the pitch-surge eigenfrequency, and the wave spectrum shape seen in Fig. 3. For TLB S, the heave/pitch-surge difference frequency apparently plays less of a role; the RAO peak is around the wave peak frequency. The heave and pitch-surge eigenfrequencies are 2.9 Hz and 2.34 Hz, respectively, well outside the wave excitation frequencies. Overall, good correlation is observed up to about 1.3 Hz for all of the platforms. TLB X3

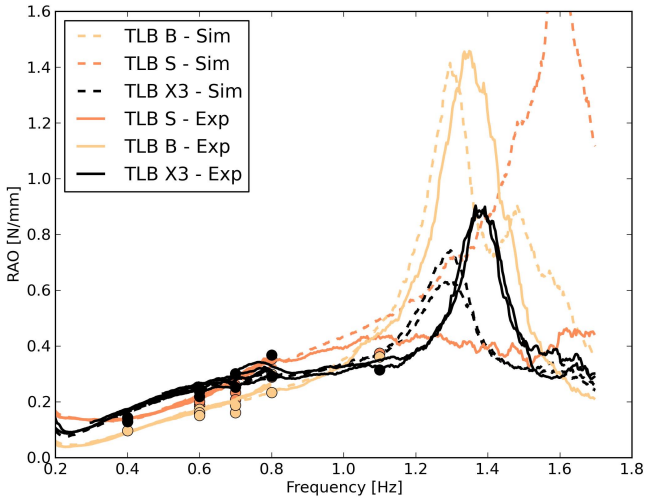

Fig. 19 RAOs for mooring line 4 (upper line, downstream direction) for all systems, with regular cases represented as dots

deviates at slightly higher frequencies than TLB B and TLB S. This is likely in connection with the offset of the peak in pitch-surge, as indicated in Fig. 15, as horizontal translation also implies a vertical component due to the mooring line configuration. The deviation at frequencies above 1.3 Hz is relatively small, as the wave excitation is close to zero. TLB S deviates at 1 Hz and above due to a combination of factors: 1) the wave excitation is low, so the uncertainty increases; 2) lack of radiation damping, which becomes more important at higher frequencies; and 3) a larger water plane area relative to the other concepts. The limited water plane stiffness for TLB X3 is also the reason for the relatively large RAO in heave, as horizontal translations induce a vertical set-down, increasing the heave motion RAO.

Overall, the mooring line forces shown in Fig. 18 and Fig. 19 are computed with high accuracy, although with a slight overestimation of RAO and small offsets on the eigenfrequencies. The exception is TLB S, where the mooring lines deviate severely above 0.8 Hz due to the double frequency response discussed in LC 9. This is consistent with the simulated results for pitch-surge and can largely be explained by the lack of high-frequency damping and the chosen strategy for integration of the hysteresis damping. After passing of waves, we observed turbulence behind TLB S. Computing and comparing accelerations from the experimental data may shed some more light on the responses for TLB S at higher frequencies. Further work is suggested on this topic.

For the upper mooring lines, the simulation provides satisfactory results for TLB S up to about 1.1 Hz, as described earlier. For TLB B and TLB X3, the simulated results are a close match in both RAO and eigenfrequencies with some offsets of the pitch-surge peaks.

CONCLUSIONS

Comparisons between the experiment and computations show overall good agreement. The differences can be explained by the modeling approach and experimental setup. The data should be well suited for further validation of numerical models.

3DFloat is able to capture heave response accurately for all of the concepts. For the pitch-surge motion, 3DFloat computes accurate results for TLB B and TLB X3. Some discrepancies are observed at higher frequencies for TLB S, but these are explained mainly by the lack of radiation damping, which is important for bodies of low mass and high water plane area, and the simplified implementation of the mooring line pulley hysteresis damping.

The upper mooring line forces are computed quite accurately for all concepts. However, the computed response of TLB S results in discrepancies above about 1 Hz. The friction in the mooring system setup likely accounts for some of this discrepancy, especially for the higher frequencies with lower excitation, and should therefore be implemented more accurately in further trials. For lower frequencies and larger excitation shown in regular LCs, 3DFloat produces high quality results, with total mooring forces deviating by less than 5% from the experimental data.

3DFloat performs very well in the area below 1 Hz, and complex multiharmonic behavior is replicated in the simulations only with minor offsets and discrepancies. Morison models are sensitive to high-frequency excitation, and it is common practice to limit excitation above three times the peak frequency for irregular wave computations (Jonkman, 2007). Detailed comparison and evaluation of all of the regular LCs is suggested in order to get a deeper understanding of the accuracy of 3DFloat for different wave conditions.

3DFloat uses generic Jonswap spectrums to compute the waves for the simulations. As the experimental trials were relatively short and therefore may not be a good representation of the spectrums, it

is suggested that simulations are run with wave component tables giving time-accurate representations of the measured wave data.

The TLB systems used in the tests are proven to be robust and predictable, both in the experimental trials and in the simulations. The overall motions are limited, but the mooring line loads and thus the anchoring loads are high. It is important to point out that neither the floaters nor the mooring systems represent full-scale systems. The sub-optimized mooring system makes it difficult to get an indication whether the load-reducing lattice structure of TLB X3 would reduce the overall costs.

ACKNOWLEDGEMENTS

We gratefully acknowledge the funding of the wave tank test and the computations by the MARINET and NOWITECH projects, NMBU, and IFE.

REFERENCES

Anderson, E, et al. (1990). "LAPACK: A Portable Linear Algebra Library for High-Performance Computers," *Proc 1990 ACM/IEEE Conf Supercomput*, New York, NY, USA, IEEE Computer Society Press, 2–11.

Copple, RW, and Capanoglu, C (2012). "Tension Leg Wind Turbine (TLWT) Conceptual Design Suitable for a Wide Range of Water Depths," *Proc 22nd Int Offshore Polar Eng Conf*, Rhodes, Greece, ISOPE, 1, 396–403.

Jonkman, J (2007). *Dynamics Modeling and Loads Analysis of an Offshore Floating Wind Turbine*, Technical Report NREL/TP-500-41958, National Renewable Energy Laboratory, Golden, CO, USA.

Jonkman, J, et al. (2010). "Offshore Code Comparison Collaboration Within IEA Wind Task 23: Phase IV Results Regarding Floating Wind Turbine Modeling," Presented at *Eur Wind Energy Conf (EWEC)*, Warsaw, Poland, NREL/CP-500-47534.

Karimirad, M, and Moan, T (2013). "Stochastic Dynamic Response Analysis of a Tension Leg Spar-Type Offshore Wind Turbine," *Wind Energy*, 16(6), 953–973.

Myhr, A, and Nygaard, TA (2012). "Load Reductions and Optimizations on Tension-Leg-Buoy Offshore Wind Turbine Platforms," *Proc 22nd Int Offshore Polar Eng Conf*, Rhodes, Greece, ISOPE, 1, 232–239.

Myhr, A, and Nygaard, TA (2014). "Experimental Results for Tension-Leg-Buoy Offshore Wind Turbine Platforms," *J Ocean Wind Energy*, ISOPE, 1(4), 217–224.

Popko, W, et al. (2012). "Offshore Code Comparison Collaboration Continuation (OC4), Phase I – Results of Coupled Simulation of Offshore Wind Turbine with Jacket Support Structure," *Proc 22nd Int Offshore Polar Eng Conf*, Rhodes, Greece, ISOPE, 1, 337–346.

Robertson, AN, and Jonkman, JM (2011). "Loads Analysis of Several Offshore Floating Wind Turbine Concepts," *Proc 21st Int Offshore Polar Eng Conf*, Maui, HI, USA, ISOPE, 1, 443–450.

Robertson, A, et al. (2014). "Offshore Code Comparison Collaboration, Continuation Within IEA Wind Task 30: Phase II Results Regarding a Floating Semisubmersible Wind System," *Proc 33rd Int Conf Ocean Offshore Arct Eng*, San Francisco, CA, USA, ASME, 9B, V09BT09A012.

Roddier, D, Cermelli, C, Aubalt, A, and Weinstein, A (2010). "WindFloat: A Floating Foundation for Offshore Wind Turbines," *J Renewable Sustainable Energy*, 2(3), 033104.

Sarpkaya, T, and Isaacson, M (1981). *Mechanics of Wave Forces on Offshore Structures*, Van Nostrand Reinhold Co, 651 pp.

Spæren, A (2013). *Development and Construction of Floating Wind Turbine Models and Test Rig for Wave Tank Test*, Masters Thesis, Norwegian University of Life Sciences, Ås, Norway. Available from http://www.nb.no/idtjeneste/URN:NBN:no-bibsys_brage_43378.

Stewart, GM, Lackner, MA, Robertson, A, Jonkman, J, and Goupee, AJ (2012). "Calibration and Validation of a FAST Floating Wind Turbine Model of the DeepCwind Scaled Tension-Leg Platform," *Proc 22nd Int Offshore Polar Eng Conf*, Rhodes, Greece, ISOPE, 1, 380–387.

Tande, JOG, Merz, K, Paulsen, US, and Svendsen, HG (2014). "Floating Offshore Turbines," *WIREs Energy Environ*, doi: 10.1002/wene.130.

Vorpahl, F, et al. (2013). "Verification of Aero-Elastic Offshore Wind Turbine Design Codes Under IEA Wind Task 23," *Wind Energy*, 17(4), 519-547, doi: 10.1002/we.1588.